GCAGS JOURNAL
A Publication of the Gulf Coast Association of Geological Societies
www.gcags.org

Beyond the Bad-Water Line—A Model for the Occurrence of Brackish Water in Upper Coastal Plain Aquifers in Texas

Stephen Z. Hoff, Jr. and Alan R. Dutton

Department of Geological Sciences, University of Texas at San Antonio, One UTSA Circle, San Antonio, Texas 78249, U.S.A.

ABSTRACT

Brackish water in the Edwards aquifer in south-central Texas is hypothesized to occur in a zone of convergent flow with hydrodynamic and transient mixing mainly between hydropressured freshwater moving downdip by gravity and saline water migrating updip from depth by a geopressure drive. Another source of water and dissolved mass is upward-directed cross-formational flow into the Edwards Group. Composite plan-view maps of a potentiometric surface and total dissolved solids (TDS) document the convergence zone. Two versions of a potentiometric surface are drawn from hydraulic-head data from the freshwater and brackish-water zones and pressure data from oil and gas wells: (1) an equivalent freshwater hydraulic-head map with constant water density = 1000 kg/m^3 and (2) a point-water hydraulic-head map with variable saltwater densities assigned to each well. The hydraulic-head maps honor equipotential contours from a 2004 synoptic map of high-stand water levels in the freshwater aquifer. Pressure data from gas wells are corrected for capillarity. The TDS map uses reported analyses of chemical composition of water samples from water wells, monitoring wells, and hydrocarbon production wells, and TDS estimates calculated from resistivity well logs. A relation between TDS and specific conductance was extended from the freshwater-to-brackish-water range to include saline water with TDS >100,000 mg/L.

A hydraulic-head minimum lies downdip of the bad-water line where the lateral gradient in hydraulic head reverses and fluid pressure climbs toward geopressure at depth. Deep geopressure in the Edwards Group drives flow of saline water updip toward the freshwater aquifer. The likely source of geopressure in the Edwards Group was fluid leakage from the geopressured Cenozoic section that overlies the Edwards Group beyond the Cretaceous shelf margin. Convergent flow implies a significant amount of vertical cross-formational discharge, which otherwise is typical of confined aquifers. The conceptual model of Edwards groundwater movement might be improved by accounting for vertical flux across the confined aquifer. Convergent flow with a vertical-discharge component might be typical of brackish-water zones in other coastal-plain aquifers in the western Gulf of Mexico Basin.

INTRODUCTION

The term 'bad-water line' has been historically associated with the downdip limit of freshwater in the San Antonio segment of the Edwards aquifer in south-central Texas, at which an isopleth of total dissolved solids (TDS) of 1000 mg/L in a plan-view map defines the regulatory limits of the aquifer (Pavlicek et al., 1987; Groschen, 1994; George et al., 2011) (Fig. 1). In three dimensions, the surface where TDS = 1000 mg/L would be highly irregular, sloping, and turning (for examples in 2D vertical cross section see Lambert et al., 2010, their figures 5–8). The vertical and lateral distribution of salinity near the bad-water line is affected by factors such as permeability and porosity, recharge and pumping, aquifer stratigraphy, and faulting.

The 'bad-water line' term, however, soon may become archaic with increased interest in brackish water with TDS between 1000 and 10,000 mg/L. Whereas to date there is no widely known plan to produce brackish groundwater for desalination from the Edwards Group, brackish water is increasingly being used as an unconventional water resource (Arroyo, 2004; Karagiannis and Soldatos, 2008; Goh et al., 2016). The brackish-water zone in the Edwards aquifer might even be used for storing freshwater. New Braunfels Utilities in New Braunfels, Texas, is considering developing an aquifer storage and recovery site within the brackish-water zone of the Edwards aquifer (Draeger, 2016).

Downdip of the freshwater zone, the Edwards Group has brackish and saline waters (Groschen and Buszka, 1997; Lambert et al., 2009, 2010; Thomas et al., 2012) and petroleum hydrocarbons (Land and Prezbindowski, 1981; Galloway et al., 1983; Kosters et al., 1989). The hydrogeology of this area has been much less studied than the freshwater-bearing Edwards aquifer.

Manuscript received March 15, 2017; revised manuscript received June 27, 2017; manuscript accepted July 6, 2017.

GCAGS Journal, v. 6 (2017), p. 135–149.

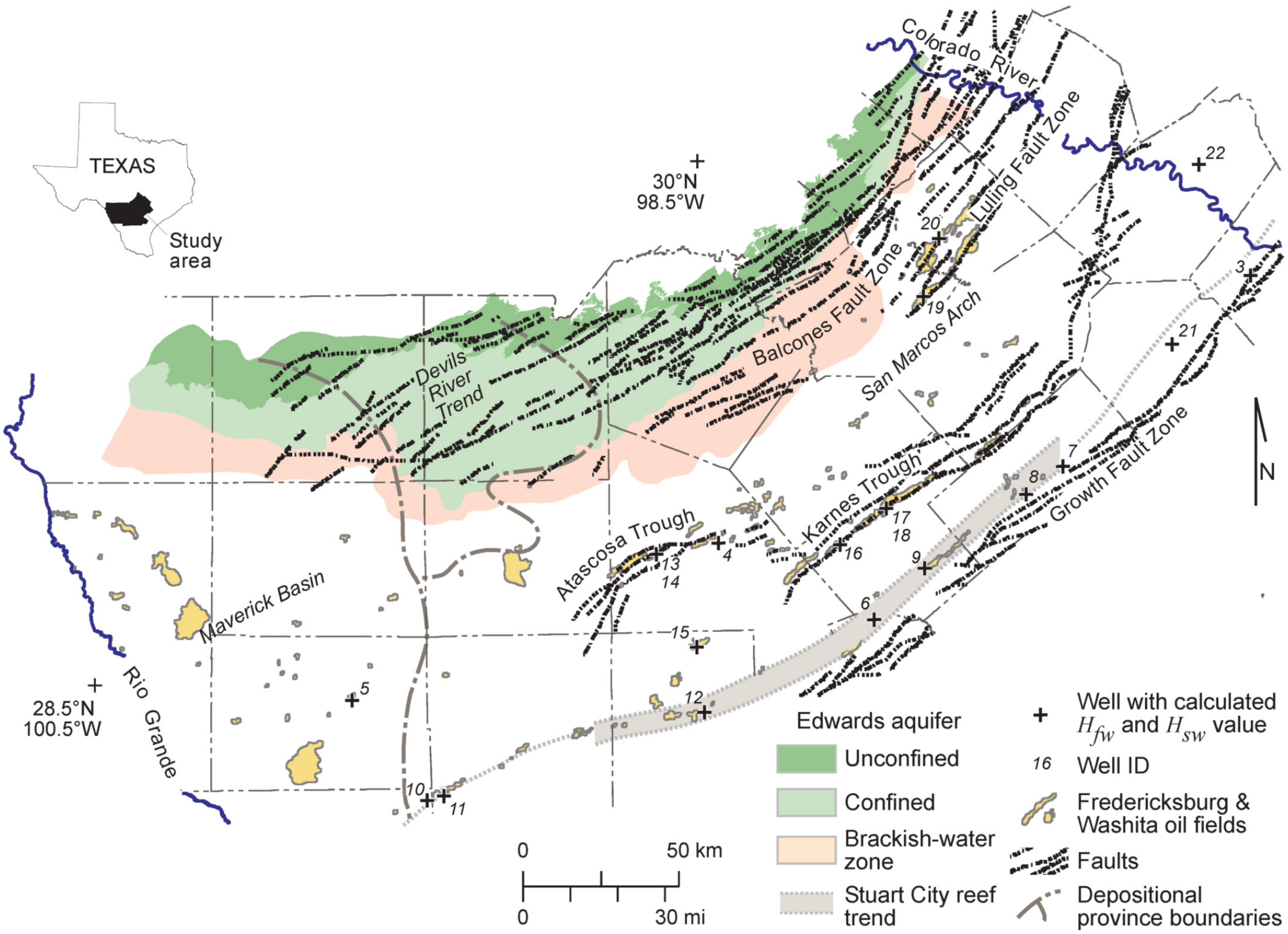

Figure 1. Map of study area showing major fault zones, depositional provinces (San Marcos Arch, Devils River Trend, Maverick Basin, and Stuart City Reef Trend), and main oil and gas fields of the Edwards Group and variations in salinity in the Edwards aquifer. Total dissolved solids (TDS) of unconfined and confined parts of the Edwards aquifer is <1000 mg/L. Brackish-water zone is defined by TDS between 1000–10,000 mg/L. Downdip of brackish-water zone salinity increases to >300,000 mg/L along parts of the Stuart City Reef Trend (Fig. 4).

This study integrates data from the groundwater- and petroleum-extraction industries and provides a regional synthesis and mapping of water salinity and hydraulic head. Mapping of potentiometric surfaces across geologic basins can yield insights on regional hydrogeology, especially when integrated with information on regional variations in salinity (e.g., McNeal, 1965; Bair et al., 1985; Belitz and Bredehoeft, 1988; Bachu, 1995; Dutton et al., 2006). Interpretation of basin-scale potentiometric surfaces can be problematic, however, because of significant salinity variations (Post et al., 2007). Numerical models of flow of variable-density fluid allow studies of regional hydraulics to be posed with pressure and density terms instead of hydraulic head (e.g., Brakefield et al., 2015). Quality numerical models, nonetheless, depend on conceptual models developed from empirical data.

The main purpose of this study is to help improve conceptual models for the origin, occurrence, and movement of brackish water in the Edwards aquifer. Dutton et al. (2006) hypothesized that the position of the limit of potable water in the Carrizo-Wilcox aquifer in Central Texas is influenced by the convergence of meteoric water flowing downdip from the aquifer's recharge area and saline formation water moving updip from the geopressured zone in the deep Gulf of Mexico Basin. This study is designed to check whether this hypothesis might apply to the Edwards aquifer. It is possible that the flow-convergence model also could explain the origin and occurrence of brackish water in other coastal plain aquifers in Texas.

STUDY AREA

The study area includes the San Antonio segment of the Edwards (Balcones Fault Zone) aquifer and its equivalent downdip rocks where brackish, saline, and brine waters and petroleum hydrocarbons occur (Fig. 1). The study area is bounded to the north-northwest by the outcrop of the Edwards Group, where the Edwards aquifer is unconfined, and to the south-southeast by the buried Stuart City Reef Trend, which marks the edge of the broad Lower Cretaceous carbonate platform and basin margin (Rose, 1972). The Colorado River and Rio Grande bound the study area to the northeast and southwest, respectively.

The Edwards Group is a suite of Lower Cretaceous (Albian) carbonate rocks that were deposited on a broad shelf or platform at the northwestern margin of the ancestral Gulf of Mexico. The San Marcos Arch, Devils River Trend, Maverick Basin, and Stuart City Reef Trend (Fig. 1) are depositional provinces within this platform setting (Lozo and Smith, 1964; Rose, 1972; Groschen and Buszka, 1997). Edwards Group stratigraphy in these areas is well documented and consists of above and below wave-base carbonate platform and reefal facies (Lozo and Smith, 1964; Rose, 1972; Bebout and Loucks, 1974; Hovorka et al., 1994, 1996; Maclay, 1995; Groschen and Buszka, 1997). The Edwards Group is overlain by the Lower Cretaceous Del Rio Clay, a hydrological confining unit, and is underlain by the Lower Cretaceous Glen Rose Formation, which hosts part of the Trinity aquifer (Jones et al., 2011). Thickness of the Edwards Group varies across the study area from generally >100 m (>330 ft) in the freshwater-bearing section to 200 to 300 m (~650 to ~1000 ft) in the saline-water zone. The ~700 m (~2300 ft) thick Stuart City Reef Trend marks the shelf edge during deposition of both the Edwards Group and underlying Glen Rose Limestone (Bebout and Loucks, 1974).

The dominant structural feature in the area is the Balcones Fault Zone (BFZ) (Figs. 1 and 2), marked by a series of en echelon, generally northeast-striking, down-to-the-coast normal faults that separate the uplifted Edwards Plateau to the north-northwest from the subsiding Gulf of Mexico Basin to the south-southeast (Ferrill et al., 2004). Balcones faults can individually exhibit throw of tens to >350 m (30 to >1150 ft), and at some locations completely displace the aquifer (Rose, 1972; Maclay, 1995; Johnson and Schindel, 2008). Edwards Group crops out ~150 to >300 m (~490 to >1000 ft) above sea level across the north-northwest side of the study area. The Edwards Group dips southeast toward the Gulf of Mexico at ~65 m/km, and at the Stuart City Reef Trend is buried under the coastal plain to depths of ~4300 m (~14,000 ft) (Fig. 1).

Three other major fault systems are subparallel the Balcones Fault Zone in the study area. The Luling Fault Zone (LFZ) sits ~40 km (~25 mi) southeast of the Edwards outcrop (Figs. 1 and 2). Luling faults, which have ~140 m (~460 ft) of throw, are antithetic to Balcones faults and trap the shallowest known, 'updip' oil deposits in the Edwards Group (Rose, 1972; Galloway et al., 1983). Both the Balcones and Luling fault zones were active in the middle to late Tertiary (Rose, 1972).

The Karnes-Atascosa Fault Zone (KAFZ) includes ~5 km (~3.1 mi) wide grabens that together laterally extend nearly 150 km (~90 mi) and lie less than 20 km (<12.5 mi) from the ancestral shelf margin (Figs. 1 and 2). The origin of this fault zone, and that of the Mexia-Talco Fault Zone to the north, is related to the movement of underlying Jurassic salt (Jackson, 1982). Salt deformation and graben subsidence continued with late deposition of the Edwards Group (Rose, 1972; Jackson, 1982); Edwards Group thickness locally is up to 50 m (<165 ft) greater within the troughs. Faulting affected formation thickness inside the graben system at least through Upper Cretaceous strata (Billingsley et al., 2016). The upthrown, coastward sides of the graben system trap the deepest oil reserves in the Edwards Group, as well as gas reserves. The majority of Edwards gas reserves, however, are found in fields extending across the Stuart City Reef Trend (Galloway et al., 1983; Kosters et al., 1989).

A growth fault zone (GFZ) occurs basinward of the Stuart City Trend (Fig. 1), where Cenozoic deposits prograded beyond the Cretaceous shelf edge (Ewing 1990; Galloway, 1982, 2001; Galloway et al., 1982). Growth faults are listric faults in which displacement increased contemporaneous with sedimentation and loading. The faults die out in basinal shale as fault-plane dip decreases.

Diagenesis has changed porosity and permeability of rocks in the Edwards Group (Prezbindowski, 1981; Maclay and Small, 1984; Mench-Ellis, 1985; Hovorka et al., 1995). Dissolution of limestone and evaporites by circulating groundwater in the unconfined and confined parts of the aquifer resulted in extensive karstification (Maclay and Small, 1984; Hovorka et al., 1995, 1998; Schindel and Gary, in press). Dedolomitization, the complete or partial transformation of dolomitic rock (dolostone) into calcite (Evamy, 1967), can enhance porosity and permeability in the confined freshwater and saline parts of the Edwards Group (Land and Prezbindowski, 1981; Mench-Ellis, 1985). High permeability on both sides of the freshwater-saline water interface (bad-water line) might be the result of mixing when freshwater displaces saline water (Hovorka et al., 1995, 1998). Some karstification, especially in the deep section, might have been driven by sulfuric acid derived from H_2S discharged from the geopressured zone or associated with migration of hydrocarbons (Jagnow et al., 2000; Schindel and Gary, in press). The extent

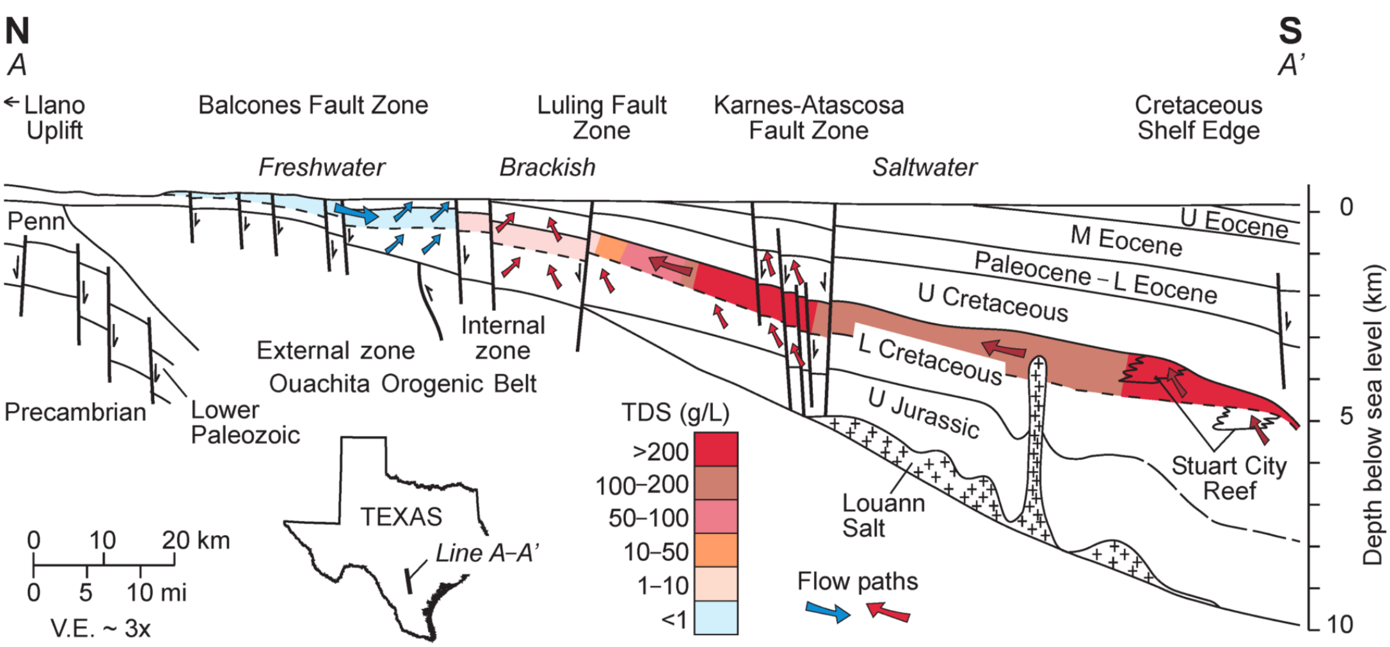

Figure 2. Vertical cross section showing generalized stratigraphy, fault zones and other structure, range of total dissolved solids (TDS in g/L) in the Edwards Group, and conceptual model of groundwater flow paths across the Edwards Group (modified after Ewing, 1991). The formations that make up the Edwards aquifer lie in the upper part of the Lower Cretaceous section. The Glen Rose and other Lower Cretaceous formations underlie the Edwards Group. The Stuart City Reef Trend lies along the Lower Cretaceous shelf margin and includes reefal deposits of both the Glen Rose Formation and Edwards Group.

and style of karstification in the brackish-water and saline zones has not been extensively studied because of limited subsurface data.

Recharge to the Edwards aquifer averages ~760 million m^3/yr (~620,000 ac-ft/yr), and occurs through (1) losing streams that cross the outcrop, (2) direct precipitation over the recharge zone, and (3) cross-formational flow from the underlying Glen Rose Formation, whether the cross-formational flux predominantly has a horizontal or vertical component (Lindgren et al., 2004; Fratesi et al., 2015). Water moves from the recharge zone downdip into the confined section of the aquifer. Regional flow within the confined Edwards aquifer, volumetrically focused through karst conduits (Worthington, 2003), is eastward toward the major artesian Comal and San Marcos springs. Discharge primarily occurs by spring flow and withdrawal from wells; their proportions of total discharge have varied through time (Lindgren et al., 2004).

The flux of groundwater moving into and out of the saline and brackish-water zones is poorly defined (Land and Prezbindowski, 1981; Maclay, 1995; Groschen and Buszka, 1997; Brakefield et al., 2015). There is no fault 'barrier' controlling the interface between the freshwater and saline-water zones along most of the bad-water line west of Comal and San Marcos springs (Schultz, 1993; Hovorka et al., 1995, 1998; Johnson and Schindel, 2008). Some amount of brackish-to-saline water might discharge into the freshwater aquifer, particularly along fault boundaries where hydraulic head on the saline-water side is higher than head on the freshwater side. Whether such updip-directed flow of brackish-to-saline water could be increased by drawdown at well fields in the freshwater aquifer has long been an environmental concern (Pavlicek et al., 1987), and led to the installation of several transects of monitoring wells across the interface between freshwater and saltwater zones (Pavlicek et al., 1987; Groschen, 1994; Lambert et al., 2009, 2010; Thomas et al., 2012).

The underlying Trinity aquifer in the Glen Rose Formation is estimated to add 0.05–0.13 km^3/yr (40,000–103,000 ac-ft/yr) of cross-formational recharge to the freshwater part of the Edwards aquifer (Lindgren et al., 2004; Jones et al., 2011). Such flux might be across both the unconfined and confined parts of the aquifer. In addition, groundwater from the Glen Rose Formation, of unknown but variable salinity, may likewise discharge to brackish- and saline-water zones in the Edwards Group (Land and Prezbindowski, 1981; Oetting et al., 1996; Groschen and Buszka, 1997). In turn, some part of the water budget of the Edwards aquifer might be discharged by upward-directed cross-formational flow through the overlying aquitard. Such regional-scale cross-formational flow is typical of confined aquifers but has not been included in previous models of groundwater flow in the Edwards aquifer (Lindgren et al., 2004; Brakefield et al., 2015; Fratesi et al., 2015). Schindel and Gary (in press) discuss hypogenic karst processes in the Edwards aquifer, including cross-formational flow.

Geopressured conditions, characterized by fluid pressure-depth gradients greatly in excess of those of hydropressured systems, are present in deeply buried Cenozoic sediments gulfward of the Lower Cretaceous shelf margin (Bethke, 1986; Kreitler, 1989; Harrison and Summa, 1991). Geopressure in the Cenozoic section is thought to be confined by shale-bounded growth faults (Jones and Wallace, 1974; Jones, 1975), the episodic rupture of which drives deep basinal fluids upward along the faults (Harrison and Summa, 1991). Harrison and Summa (1991) included the Edwards Group in a model of the origin and history of geopressure in the Gulf of Mexico Basin. Geopressure, originating within the Cenozoic section, might have built up in the deep Edwards Group by 31 million years ago (Ma), and have reached a maximum in the past 2–5 Ma (Harrison and Summa, 1991). Groschen and Buszka (1997) did not find sufficient data to confirm whether geopressure is present in the Cretaceous section in the study area.

METHODS

Mapping of Total Dissolved Solids

A composite map of salinity of groundwater in the Edwards Group, represented by total dissolved solids (TDS), was drawn by merging groundwater- and petroleum-industry datasets, following Dutton et al. (2006). This study included information on water samples from wells and estimates of TDS derived from geophysical logs, including:

(1) Data on "Total dissolved solids, sum of constituents (mg/L)," downloaded from an online database (TWDB, 2016b) for 1490 water wells in the Edwards aquifer. Average TDS was determined for repeated samples.

(2) Data for the transition from fresh to saline water (Lambert et al., 2009, 2010). There were 91 analyses of chemical composition of groundwater samples from 28 wells in the transition-zone well arrays. Nine of the samples had charge balance >5 percent and were not used. Samples with the highest TDS were selected for each well with repeated samples.

(3) Data on chemical composition for 129 samples of groundwater in the saline zone, compiled from the U.S. Geological Survey (USGS) National Produced Waters Geochemical Database (Blondes et al., 2013). This compilation included legacy data from previous studies by Land and Prezbindowski (1981) and Groschen and Buszka (1997). Four samples from Land and Prezbindowski (1981), absent from the USGS database, were also included. Sample records missing major elements or having charge-balance error >5% were excluded. Samples with grossly incorrect or missing locational data were assigned to geometric centroids of their respective fields.

(4) Estimates of TDS converted from resistivity well logs, taken from Schultz (1992, 1993) for the freshwater to slightly saline zone.

(5) Additional estimates of TDS, converted from induction-resistivity logs run in 9 oil and gas exploration wells, followed the methods of Schultz (1992, 1993). This study extended his log-linear relationship between calculated specific conductance and TDS concentration to TDS >100,000 mg/L. The pooled data define a trend consistent with that for the Schultz (1993) data alone. The regression for Schultz (1993) data lies within the confidence interval of the pooled data regression (Fig. 3).

The method used by Schultz (1992, 1993) was followed in this study both for consistency and because alternative methods for estimating water quality from borehole geophysical logs are less applicable to carbonate systems, particularly those which have significant hydrocarbon saturation (Turcan, 1966; Asquith and Krygowski, 2004; Hamlin and de la Rocha, 2015). The Schultz (1992, 1993) method is based on the Archie (1942) equation:

$$R_0 = F \cdot R_w \tag{1}$$

where R_0 is the resistivity of the formation at 100 percent water saturation, i.e., the deep resistivity reading taken from a geophysical log; R_w is water resistivity, which is resistivity of the formation water alone at formation temperature; and F is formation resistivity factor, a constant relating R_0 and R_w. R_0 and R_w are given in ohm-m. Typical fluids used for drilling oil and gas wells in the saline Edwards Group are freshwater- and oil-based muds that have low conductivity. The saline Edwards Group has high conductivity, for example, ~1400 microsiemens/cm (µS/cm). Under these conditions, the deep-resistivity reading from the induction log is assumed to approximate true formation resistivity of the noninvaded zone (Asquith and Krygowski, 2004).

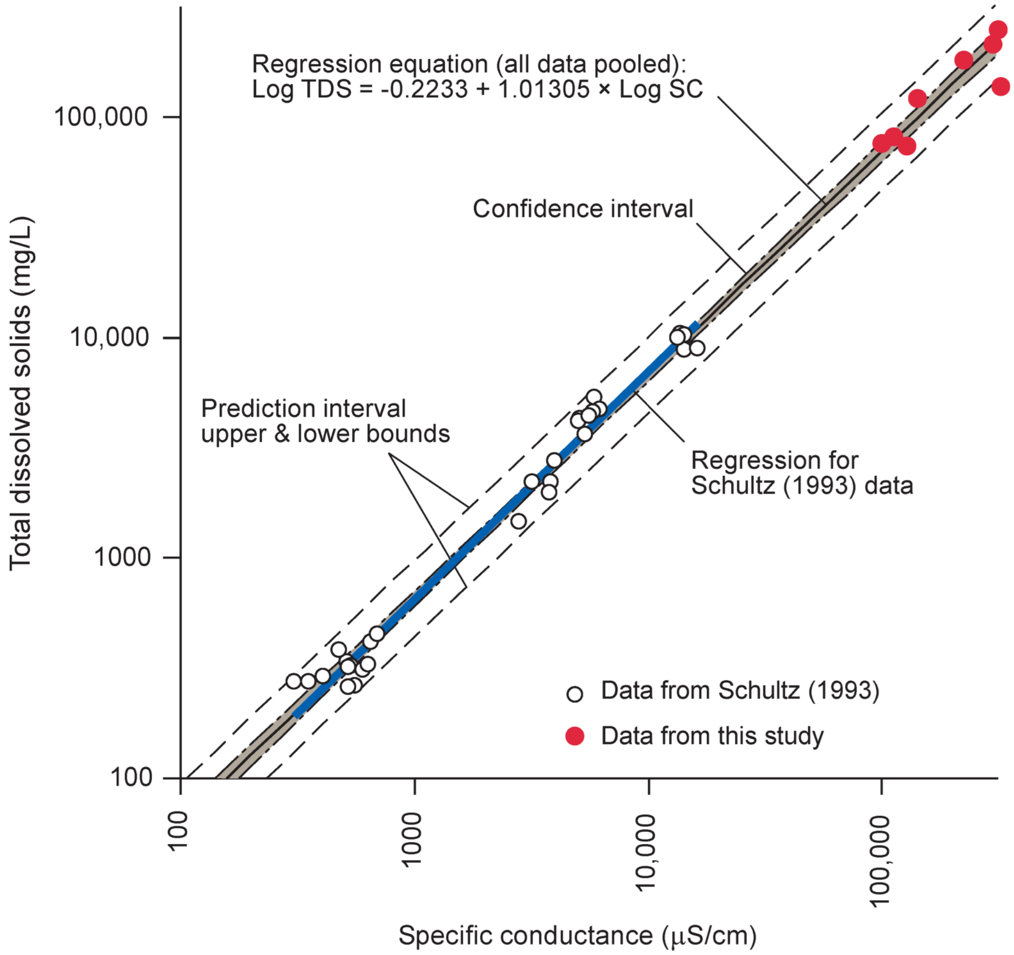

Figure 3. Calibration for prediction of total dissolved solids (TDS) from specific conductance (SC, units of microsiemens per cm [µS/cm]) calculated from geophysical logs at related wells. Bold blue line is regression for Schultz (1993) data. Prediction and confidence intervals (95 percent) for regression equation of all data pooled.

Archie (1942) related formation factor to formation porosity:

$$F = a / \varphi^m \qquad (2)$$

where a is a tortuosity factor, φ is porosity, and m is a cementation exponent that reflects grain-size distributions. Schultz (1992, 1993) used values of 1 and 2 for a and m, respectively, taken as typical for carbonate rocks (Asquith and Krygowski, 2004). These values were also used in this study.

Combining and rearranging Equations 1 and 2 gives:

$$R_w = R_0 \cdot \varphi^2 \qquad (3)$$

R_w is converted to specific conductance (SC), the electrical conductivity of a material at standard temperature (25°C [77°F]). However, R_w is first expressed at 25°C (77°F) using Arp's Formula (Schlumberger, 1974):

$$R_{w\_standard} = R_w \cdot (T_{fm} + 21) / (T_{standard} + 21) \qquad (4)$$

where $R_{w\_standard}$ is temperature-corrected water resistivity in ohm-m, T_{fm} is formation temperature, and $T_{standard}$ is temperature to which resistivity is corrected, in this case 25°C (77°F). Equation 5 converts $R_{w\_standard}$ to SC:

$$SC = 10{,}000 / R_{w\_standard} \qquad (5)$$

where SC is in µS/cm. Combining Equation 5 with Arp's Formula and substituting 25°C (77°F) for $T_{standard}$ gives:

$$SC = 460{,}000 / [R_w \cdot (T_{fm} + 21)] \qquad (6)$$

For this study, values for T_{fm} were estimated by linearly interpolating between bottom-hole temperature as recorded in the geophysical log and mean annual temperature at land surface, assumed for the study area to be 20°C (68°F) (NOAA, 2016). Additional details on the SC–TDS calculations and selection of data are included in Hoff (2016).

Mapping of Hydraulic Head

Two versions of a potentiometric surface of Edwards groundwater were mapped by combining water-level data from the freshwater aquifer and pressure data from monitoring wells in the brackish-water zone and oil and gas wells farther downdip in the saltwater zone. Inferring lateral gradients in fluid potential from such regional maps is problematic because of the range in salinity (Post et al., 2007). Interpretation of the maps, however, might indicate whether there are multiple sources of water in the Edwards Group and whether there is a reversal in hydraulic-head gradient between the water sources. Data for the maps included:

(1) Equipotential contours for the freshwater zone, taken from a synoptic water-level map for December 2004 (Hamilton et al., 2006). This map reflects a period of high water levels in the freshwater part of the aquifer. Its water-level contours incorporate interpretations of the influence of structural faulting and karst conduits on the movement of groundwater in the freshwater part of the aquifer.

(2) Values of equivalent freshwater head for the brackish-water zone, calculated from data obtained from pressure transducers in monitoring wells along multiple transects between the freshwater and saltwater zones (Lambert et al., 2010; Thomas et al., 2012). Data were taken from an online database (TWDB, 2016a).

(3) Hydraulic-head estimates for the saline zone, calculated from pressure tests and other data for oil and gas wells. Pressure data for 1970–2015 on 1358 gas wells completed in the Edwards Group were downloaded from Lasser Production Data Inc. (2015). Pressure at the first or second earliest data in >94% of wells averaged ~28 megapascals (MPa) (~4000 psi) higher than subsequent pressure values. It was assumed, therefore, that the earliest pressure data at each well were most representative of initial reservoir pressure. Data selected for mapping, however, were limited to 12 of the wells with bottom-hole pressure (P_{bh}), or shut-in well-head pressure (P_{wh}) that could be converted to P_{bh}. Ten additional mappable estimates of P_{bh} for Edwards oil and gas wells were taken from Galloway et al. (1983) and Kosters et al. (1989), respectively.

Calculating hydraulic head from qualified gas-pressure data followed several steps. First, P_{wh} was converted to P_{bh}:

$$P_{bh} = P_{wh} + [(1 - S_w) \cdot \rho_g \cdot g \cdot b] + (S_w \cdot \rho_w \cdot g \cdot b) \quad (7)$$

where S_w is water saturation, ρ_g is the density of gas, g is the acceleration due to gravity (9.81 m/sec^2), b is total thickness of the fluid column in a well, and ρ_w is the density of water (Lyons and Plisga, 2004). Equation 7 assumes hydrostatic conditions for both gas and water columns. For each datum, ρ_g was calculated from specific gravity of gas (SG_g) measured at the well head; SG_g was assumed to have been pressure and temperature corrected at the time of reading. When SG_g, or S_w, or both were absent, the arithmetic average for all 1358 data points was used (0.689 and 0.22 for SG_g and S_w, respectively). SG_g and water saturation were assumed to be unaffected by production and pressure decline, and water and gas were assumed to be the only phases present in the borehole.

Second, water pressure (P_w) was calculated by subtracting capillary pressure (P_c) from P_{bh} (Ahmed, 2006, p. 204):

$$P_w = P_{bh} - P_c = P_{bh} - b_{res} \cdot (\rho_w - \rho_g) \cdot g \quad (8)$$

Galloway et al. (1983) and Kosters et al. (1989) give thicknesses of the gas column (b_{res}) for specific Edwards oil and gas reservoirs. An average b_{res} was used for wells in other Edwards reservoirs.

Hydraulic head (Hw) was calculated by:

$$H_w = z + P_w / (\rho_w \cdot g) \quad (9)$$

where z is the elevation of the P_{bh} measurement, relative to the sea-level datum. Elevation (z) for P_{bh} was found by subtracting measurement depth from an estimate of land-surface elevation for each well obtained from digital ground-surface elevation data with 10 m (~33 ft) vertical resolution (USGS, 2013). Elevation ranged ~4300 m among the 22 mappable wells.

Two potentiometric-surface maps were made. One is an equivalent freshwater-head version with ρ_w =1000 kg/m^3 in Equations 7–9. The second version used a variable ρ_w, interpolated from the TDS map, as follows. Log$_{10}$TDS values of digitized contours and additional control points were gridded by kriging in Golden Software Surfer® version 8. Root mean square error of TDS, comparing values for measured and interpolated values at 40 control points in the saline zone, was ~6700 mg/L, which was 2.2% of the range in TDS for these data. TDS interpolated at each of the 22 mappable wells was then converted to density using an empirical, statistically significant relation between water-sample data on ρ_w and TDS (Blondes et al., 2013):

$$\rho_w \text{ (kg/m}^3) = 1000 \cdot (7.17033 \times 10^{-7} \cdot TDS \text{ (mg/L)} + 1.00112195) \quad (10)$$

The regression has a correlation coefficient (r) = 0.997, sample size (n) = 117, and standard error (s_e) = 0.00359. The ρ_w estimates for the 22 wells range from 1006 to 1228 kg/m^3.

Hydraulic head calculated with Equation 9 using ρ_w unique for each mappable well might be considered a point-water head (Lusczynski, 1961; Post et al., 2007). The interpolated ρ_w value represents a vertical average outside of the well at its well screen rather than point densities inside the well (Post et al., 2007). Data used in Equations 7–9 for calculating hydraulic head are given in Table 1.

Spatial coordinates for wells without locational data were assigned to geometric centroids of their respective fields using ArcMap® version 10.2 and a map of oil and gas fields in the Edwards Group digitized from GEOMAP (1979). Hydraulic-head data for the brackish-water and saltwater zones was contoured manually and integrated with the Hamilton et al. (2006) equipotentials for the freshwater section. Additional details on data analysis, calculations, and contouring used in this study are included in Hoff (2016).

RESULTS

Salinity increases from 1000 to 10,000 mg/L across the brackish-water zone at rates of ~600 mg/L/km [~970 mg/L/mi] in the central part of the study area (Fig. 4). This is ~3x higher than the salinity gradient in the freshwater zone. The brackish-water zone is largely absent, however, in the eastern part of the study area, where BFZ faulting appears to impede flow between updip and downdip sections of the aquifer (Thomas et al., 2012). TDS increases to >200,000 mg/L in the saline zone. Highest TDS overlies the Atascosa and Karnes troughs and along parts of the Stuart City Reef Trend (Figs. 1 and 2). The TDS gradient in the saline zone is 2000–2400 mg/L/km (3220–3860 mg/L/mi) (Fig. 4).

The position of the 1000 mg/L contour (bad-water line) (Fig. 4) locally differs from that of Schultz (1992, 1993) because this study used a different geophysical-log interval for estimating the representative TDS in a well, and recent TDS measurements from wells near the freshwater-saline water interface (Lambert et al., 2009; Thomas et al., 2012; TWDB, 2016b). Schultz (1992, 1993) selected an interval having the lowest TDS to define each well's representative TDS; the resulting map showed the greatest extent of available freshwater in the aquifer. Given the possibility that some Edwards Group sections in the saline zone have hydrocarbons, which usually occur in the upper part of the section, this study calculated TDS for the bottommost interval for all wells, to avoid the complication of factoring out the effect of hydrocarbons on the resistivity-log signal. Average TDS for bottom intervals is ~2000 mg/L greater than for uppermost intervals in brackish-water-zone wells included in Schultz (1992, 1993).

Pressure data for Edwards groundwater in the study area appear to lie in several pressure regimes (Fig. 5):

(1) Data from the freshwater zone and updip part of the brackish-water zone, to depths of several hundred meters, plot along a typical hydropressured freshwater line (Fig. 5, line 1) with a pressure-depth gradient of 9.8 MPa/km (0.434 psi/ft) (Kreitler, 1989).

(2) Most of the 22 mapped oil and gas data in the saline zone (12 from Lasser Production Data Inc. [2015] and 10 from Galloway et al. [1983] and Kosters et al. [1989]), at depths of 2000–4000 m (6550–13,100 ft), have an apparent hydrostatic pressure-depth gradient >10 MPa/km (0.442 psi/ft) and 12 have pressure-depth gradient >11 MPa/km (0.486 psi/ft) (Fig. 5). Most samples' pressure-depth ratio is less than the sublithostatic gradient of ~15.8 MPa/km (0.7 psi/ft). These pressures are greater than one would expect from a hydrostatic column of saline water extending from the measurement depth to ground surface (Fig. 5,

Table 1. Parameters for calculation of hydraulic head using Equations 7–9. 1 MPa = ~145 psi and 1 m = ~3.28 ft.

Well ID	Source*	b (m)	ρ_w (kg/m^3)	SG_g	S_w	P_{wh} (MPa)	ρ_g (kg/m^3)	b_{res} (m)	P_c (MPa)	P_{bh}** (MPa)	P_w** (MPa)	z (m)	H_{fw} (m)	H_{sw} (m)
1†	1	3658	1110.9	0.696	0.19	25.51	0.85	30	0.29	33.08f 33.81s	32.78f 33.52s	-3554	-208	-478
2††	1	2743	1228.0	0.631	0.22	30.58	0.77	30	0.29	37.01f 38.34s	36.72f 38.05s	-2574	1173	585
3	1	4938	1113.5	0.659	0.76	42.75	0.81	30	0.29	80.05f 84.16s	79.76f 83.87s	-4842	3297	2836
4	1	2338	1157.0	0.669	0.22	18.95	0.82	30	0.29	24.45f 25.23s	24.16f 24.94s	-2211	255	-13
5	1	2743	1006.4	0.669	0.22	24.52	0.82	30	0.29	30.98f 31.00s	30.69f 30.71s	-2576	556	536
6	1	4267	1182.9	0.630	0.22	38.83	0.77	30	0.29	48.09f 50.50s	47.80f 50.20s	-4115	763	212
7	1	4432	1162.7	0.650	0.04	50.33	0.80	30	0.29	52.93f 53.18s	52.64f 52.89s	-4374	997	263
8	1	4466	1169.3	0.669	0.22	42.85	0.82	30	0.29	53.37f 54.98s	53.08f 54.69s	-4368	1049	400
9	1	4290	1169.6	0.669	0.22	40.44	0.82	30	0.29	50.55f 52.09s	50.25f 51.80s	-4210	918	305
10	1	3353	1227.5	0.672	0.58	27.23	0.82	30	0.29	46.81f 51.13s	46.51f 50.83s	-3193	1553	1028
11	1	3353	1221.4	0.670	0.48	25.86	0.82	30	0.29	42.12f 45.58s	41.83f 45.29s	-3197	1072	583
12	1	3810	1036.4	0.665	0.03	29.23	0.81	30	0.29	41.40	41.10	-3704	491	340
13	3	2225	1128.3	0.835			834.81	122	0.20	23.78	23.58	-2067	340	64
14	2	2245	1128.3	0.669			0.82	11	0.10	23.78	23.68	-2087	329	52
15	2	3093	1105.9	0.669			0.82	10	0.10	33.95	33.85	-3001	454	120
16	2	3328	1059.5	0.669			0.82	9	0.09	33.10	33.01	-3226	143	-50
17	3	3307	1062.2	0.825			825.07	37	0.06	35.87	35.81	-3207	447	230
18	2	3290	1062.2	0.669			0.82	9	0.09	35.85	35.76	-3190	459	242
19	3	792	1017.0	0.845			844.78	61	0.09	8.27	8.18	-632	203	188
20	3	671	1012.3	0.845			844.78	46	0.07	9.65	9.58	-526	452	439
21	2	4011	1112.8	0.669			0.82	41	0.40	49.36	48.96	-3931	1065	554
22	2	3358	1031.5	0.669			0.82	23	0.22	42.05	41.83	-3207	1062	927

* Source: 1–Lasser Production Data Inc. (2015), 2–Kosters et al. (1989), and 3–Galloway et al. (1983).

** Where applicable, values for freshwater (f) and saltwater (s) are given by the first and second terms, respectively.

† Not posted or contoured as low value is suspected to be incorrect or extremely affected by pressure drawdown.

†† Not shown; location is outside of study area.

Columns: b, total thickness of fluid column; ρ_w, water density; SG_g, specific gravity of gas; S_w, water saturation; P_{wh}, shut-in well-head pressure; ρ_g, gas density; b_{res}, reservoir height; P_c, capillary pressure; P_{bh}, bottom-hole pressure; P_w, water pressure; z, elevation of pressure measurement (mean sea level datum); H_{fw}, calculated freshwater head; and H_{sw}, calculated point-water (saltwater) head. H_{fw} uses ρ_w = 1000 kg/m^3 in Equations 7–9; H_{sw} uses ρ_w as listed in table.

Notes: (1) Data sources provided P_{bh} for wells 13–22; Sw and P_{wh} not calculated in this study. (2) Fluid density (ρ_o, not ρ_g) for oil column in wells 13, 17, and 19–20. (3) Accuracies of H_{fw} and H_{sw} most likely are no better than ±5 m (±16.4 ft) owing to unknown measurement errors in calibration and estimated depth of pressure gauges, well deviation from vertical, accuracy of fluid densities, etc.

lines 2–5). Most of the samples in this study have TDS <200,000 mg/L. Under hydrostatic conditions, most values should plot to the left of line 4.

(3) Many of the water pressures (P_w in Equation 8) calculated from gas wells have an apparent hydrostatic pressure-depth gradient less than that of freshwater (9.8 MPa/km [0.434 psi/ft] for 1000 mg/L water). Although the earliest pressure data were used from each well, reservoir pressure might have decreased owing to earlier production in those gas fields. If there had been no depletion, hydrostatic pressures in the saltwater zone should plot between line 2 (pressure-depth gradient of ~9.9 MPa/km [0.438 psi/ft], equivalent to that for water with TDS of 10,000 mg/L) and line 6 (sublithostatic gradient of ~15.8 MPa/km [0.698 psi/ft]). The mappable data from Lasser Production Data Inc. (2015) represents a sample of this population, selected because bottom-hole pressure (P_{bh}) or shut-in well-head pressure (P_{wh}) were reported. These data, and likely also those from Galloway et al. (1983) and Kosters et al. (1989), also might include pressure-drawdown effects of fluid production.

(4) Some data with the highest fluid pressure (P_w) for mapped and unmapped samples between depths of 2800–5200 m straddle the sublithostatic gradient line of ~15.8 MPa/km (0.698 psi/ft). Data with the highest pressure-depth ratios come from wells in the Stuart City Reef Trend. The highest individual values, 16.8 MPa/km (0.743 psi/ft) and 14.3 MPa/km (0.633 psi/ft), are found at depths of ~2700 m (8860 ft) and ~4800 m (15,750 ft) at the eastern and western extremities of the trend, respectively. Not all of the

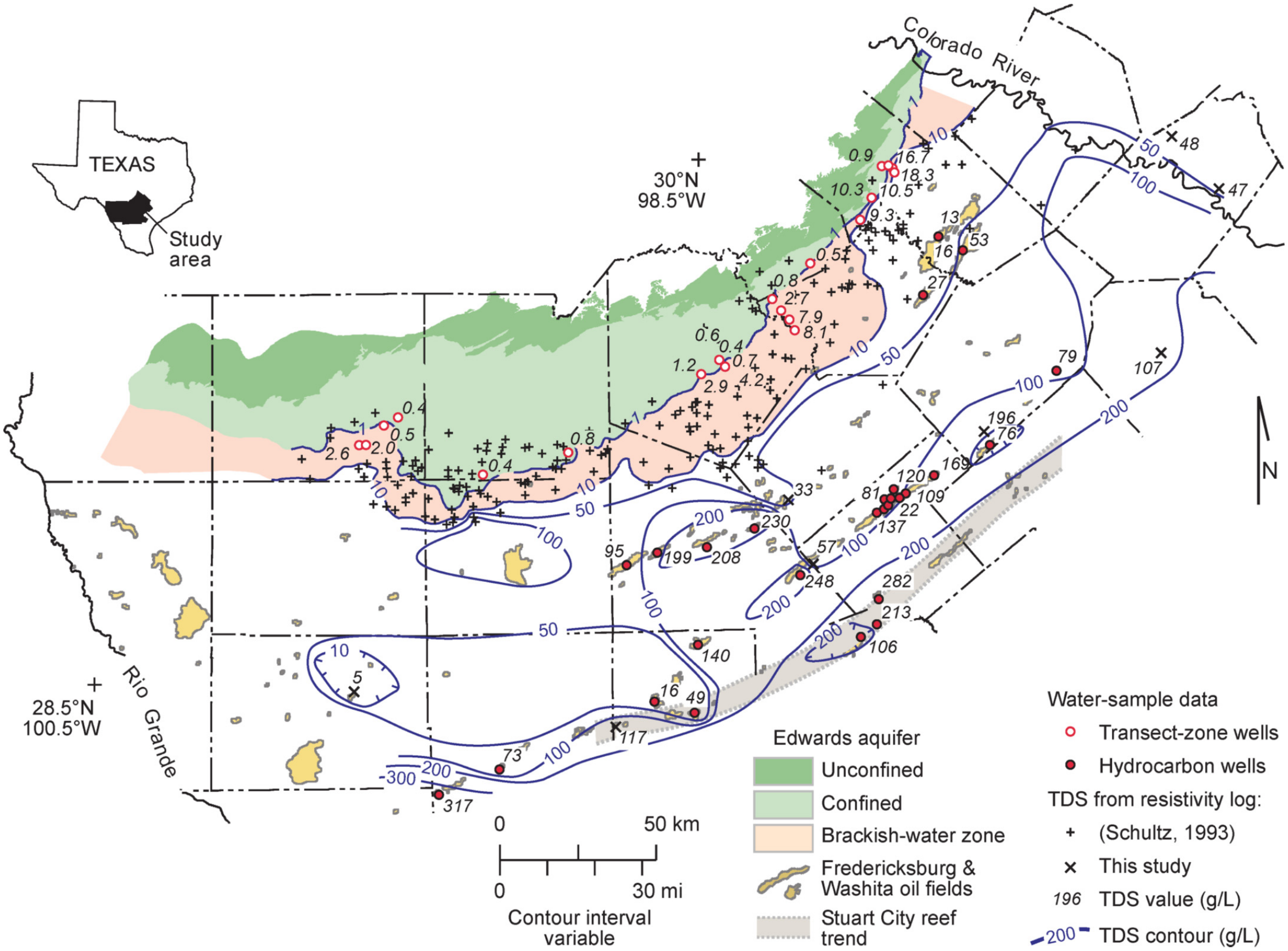

Figure 4. Map of total dissolved solids (TDS) for the brackish- and saline-water zones of the Edwards Group. TDS = 1 g/L defines the downdip limit of freshwater in the Edwards aquifer. Brackish-water zone is defined by TDS between 1000–10,000 mg/L.

wells along the Stuart City Reef Trend have very high hydraulic heads (Figs. 6 and 7).

Distribution of hydraulic head in the freshwater aquifer (Fig. 6) is well known: highest to the northwest, decreasing to the south-southeast from the outcrop into the confined section of the aquifer, and further decreasing eastward toward Comal and San Marcos springs (Hamilton et al., 2006). Hamilton et al. (2006) contoured hydraulic head separately for the unconfined and confined zones. The horizontal gradient in hydraulic head in the freshwater zone is small and typical of that of confined highly transmissive aquifers, ranging from ~0.002 in the western part of the aquifer to ~0.0005 in the eastern part.

Combining hydraulic heads for the freshwater section with heads for the brackish-water and saltwater zone give different impressions of a potentiometric surface depending on whether Equations 7–9 use water density (ρ_w) = 1000 kg/m^3 (equivalent freshwater head, Fig. 6) or a variable ρ_w related to salinity at each well (point-water head, Fig. 7). The two versions of a potentiometric surface have some similar features:

- Hydraulic-head contours in both composite maps suggest that the 190-m hydraulic-head contour is closed around Comal and San Marcos springs (Figs. 6 and 7) where ρ_w is relatively small. The 200-m contour also might appear closed if additional data for the brackish-to-saline zone were available to the northeast.
- Both maps have highest heads in the eastern and southwestern parts of the saltwater zone. Equivalent freshwater heads are, of course, higher than point-water heads, but both maps show steep increases in head to the east and southwest.
- In both maps, hydraulic head is lower in the central part of the Stuart City Reef Trend in the study area than to the northeastern and southwestern parts of the saltwater zone.

Two several significant differences between the two maps of the potentiometric surface are:

- Point-water equipotential contours (Fig. 7) are closed around oil and gas fields in the Atascosa Trough and Karnes Trough (KAFZ). Point-water heads in those oil fields are at sea level ±50 m. Only one well in that area has a low equivalent freshwater head (#16, H_{fw} = 143 m, Table 1) that requires closed contours (Fig. 6).
- An apparent minimum in hydraulic head and reversal in apparent hydraulic-head gradient roughly corresponds to the TDS = 10,000 mg/L isopleth in the map of equivalent freshwater head (Fig. 6). The apparent minimum follows the TDS = 10,000 mg/L isopleth in the west and northeast, but runs through the Atascosa and Karnes troughs in the central part of the study area in the map of point-water heads (Fig. 7).

One issue that has not been addressed is the effect of fluid movement across grabens in the KAFZ. Edwards reservoirs in the Atascosa and Karnes troughs are downthrown relative to the structure of the rest of the Edwards Group across the saltwater

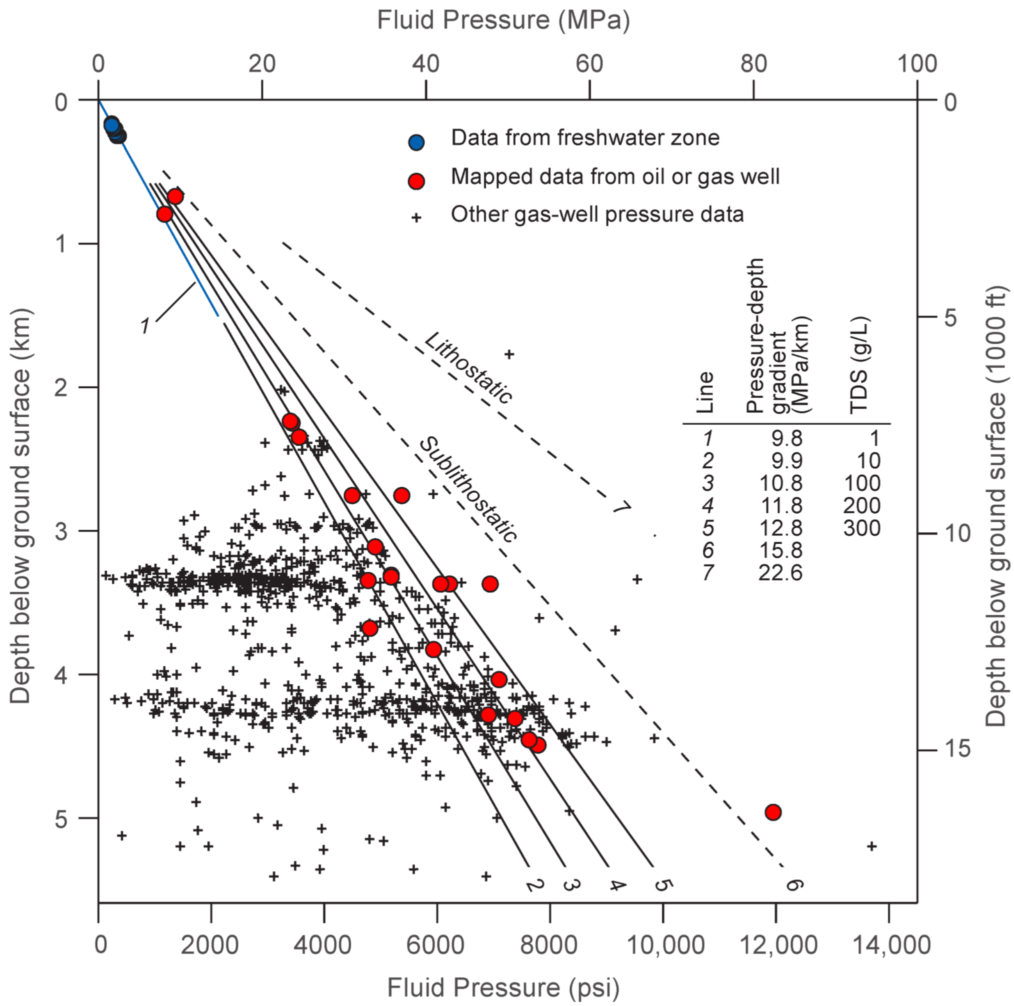

Figure 5. Graph of calculated fluid pressure (P_w, units of MPa) versus depth below ground surface for Edwards oil and gas wells and selected groundwater wells. Lines: 1, hydrostatic freshwater (TDS <1000 mg/L); 2–5, hydrostatic columns of fluid density corresponding to TDS of 10–300 g/L; 6, sublithostatic; and 7, lithostatic.

zone. TDS data (Fig. 4) are contoured to emphasize the local effects of the fault zone (Fig. 2). Apparent drawdown in point-water head (Fig. 7) might be influenced by bounding faults and offset of Edwards reservoirs against less permeable rocks.

DISCUSSION

The empirical data presented in the pressure-depth plot (Fig. 5) and maps of salinity and hydraulic head (Figs. 4, 6, and 7) raise at least 4 questions. Additional data and study are needed to develop well-tested answers. The following discussion summarizes the scientific issues posed by these questions.

(1) What is the Origin of the Brackish-Water Zone?

Two alternate models for the origin of brackish water in the Edwards Group are: (1) an increasing TDS owing to water-rock reaction along deeply circulating flow paths, and (2) mixing of two or more groundwaters with differing TDS values. Water-rock reaction and hydrogeologic properties suffice to explain TDS increase from a few hundred mg/L to 1000 mg/L (Fig. 4) in the freshwater aquifer (Sharp, 1990). Pearson and Rettman (1976), for example, showed that saturation indices for calcite and dolomite were less in the recharge zone than in the confined part of the freshwater aquifer, and were at saturation in the saline zone. Hovorka et al. (2004) suggested that variation in TDS within the freshwater section can be used to map conduit zones which have faster flow rates and shorter residence time of water.

It might be possible for further rock-water reaction to increase TDS greater than 1000 mg/L in the upper part of the brackish-water zone. Rock-water reaction, however, does not likely account for increase in TDS to >200,000 mg/L beyond the brackish-water zone (Fig. 4). Groschen and Buszka (1997) argued that groundwater in the saline section is compartmentalized, separate from the freshwater aquifer, and has a distinct chemical composition. Land and Prezbindowski (1981) proposed that the chemical and isotopic composition of saline waters in the Edwards Group is best explained by mixing of groundwaters, including vertical discharge of basinal Na−Ca−Cl brine upward along fault zones into the saline section of the Edwards Group. Oetting et al. (1996) interpreted mixing of multiple waters within the saline Edwards section, including basinal brine and Trinity Group groundwater or varying chemical composition. Land and Macpherson (1992) argued that brines in the overlying Cenozoic section were derived from dissolution of halite by old meteoric water in the Mesozoic section followed by further rock-water reaction at elevated temperature at depth.

We surmise, therefore, that the brackish-water zone is most likely explained by the mixing of two or more groundwaters of varying salinity, including but not limited to freshwater and saline water within the Edwards Group and upward-directed cross-formational flow from the Trinity Group.

(2) What is the Mechanism Driving Saline Water Updip from the Deep Edwards Group?

The equivalent freshwater head (Fig. 6) and point-water head (Fig. 7) versions of the potentiometric surface differ mainly in rendering low hydraulic heads in the Atascosa and Karnes troughs and in the location of a hydraulic-head minimum. The

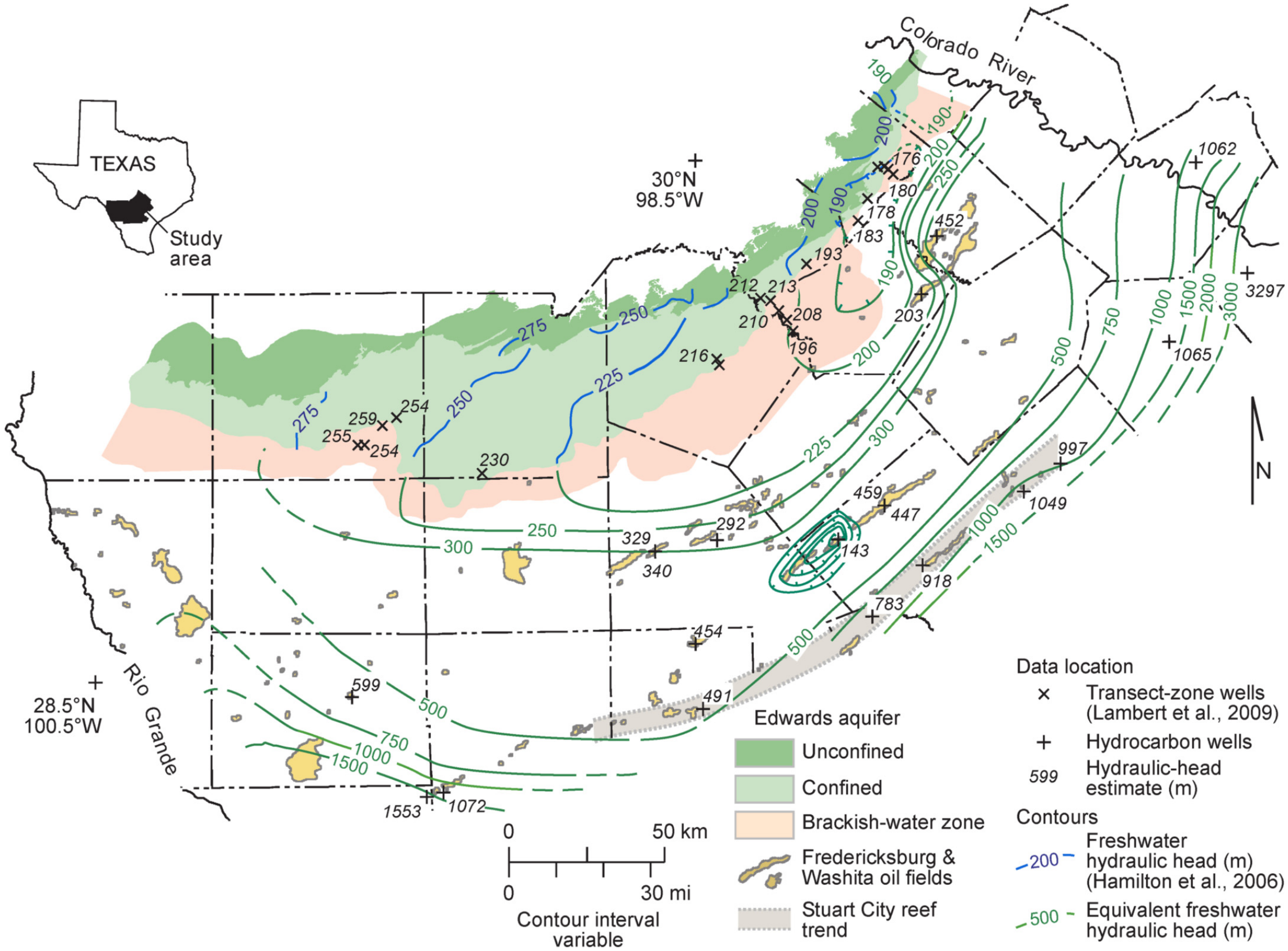

Figure 6. Map of potentiometric surface for the Edwards Group using equivalent freshwater head. Equivalent freshwater hydraulic head for brackish-water and saltwater zones uses ρ_w = 1000 kg/m^3 in Equations 7–9. Variable contour interval selected to merge equipotential lines in freshwater zone with those in brackish-water and saltwater zones. 1 m = ~3.28 ft.

differences illustrate the need to appropriately account for fluid density in regional mapping of hydraulic head (Post et al., 2007). One explanation for the point-water head version (Fig. 7) is that it more correctly renders the effect of pressure drawdown owing to production of oil and gas (and co-produced formation water) in fields along the Atascosa and Karnes troughs. Both versions of the potentiometric surface, therefore, might be interpreted as representing a transient, post-development feature. Available data do not suffice to capture the predevelopment potentiometric surface, in spite of earliest pressure data being used for each well.

The pressure-depth diagram and maps of hydraulic head indicate very high fluid pressure at depth in the Edwards Group and especially along northeastern and southwestern parts of the Stuart City Reef Trend (Figs. 5–7). The pressure-depth ratios of the highest fluid pressures for mapped data (Fig. 5) are consistent with those documented at the top of the geopressure zone in Cenozoic sections (Jones and Wallace, 1974; Jones, 1975; Dutton et al., 2006). In the Cenozoic formations, 'transitional' pressures might indicate an intercept of multiple sublithostatic gradients (Jones and Wallace, 1974; Jones, 1975; Leftwich and Engelder, 1994). Results of the Harrison and Summa (1991, their figure 15) model show geopressure extending into the rocks of the Lower Cretaceous shelf by 31 Ma. Dutton et al. (2006) hypothesized that saltwater episodically enters the saline zone of one coastal plain aquifer when fluid pressure at greater depth approaches the lithostatic gradient and growth faults open. The hydraulic-head gradient across the saltwater zone might reflect a transient decay in pressure with distance updip from the growth fault zone.

Hydraulic head is higher in saltwater-bearing fault blocks than in the updip freshwater-bearing fault blocks near Comal and San Marcos springs (Lambert et al., 2009; Thomas et al., 2012). Additional study is needed to evaluate the origin of high head in updip saltwater-bearing fault blocks. High head might not be explained with a 3D model of gravitationally driven flow of recharged meteoric water, but could require an updip-directed drive of formation water, with a distal, downdip geopressured fluid source.

Geopressured conditions in the deep Edwards Group might provide an updip-directed fluid drive, similar to that described by Dutton et al. (2006) for the Carrizo-Wilcox aquifer in central Texas. Informal queries among geologists who have worked in Edwards oil and gas fields, however, have not yielded first-hand confirmation that Edwards fluid pressure is high enough to warrant caution during well drilling and completion. Geopressure has not been confirmed, therefore, although gas pressure calculations and numerical modeling (Harrison and Summa, 1991) suggest it might have occurred in the deep Edwards Group.

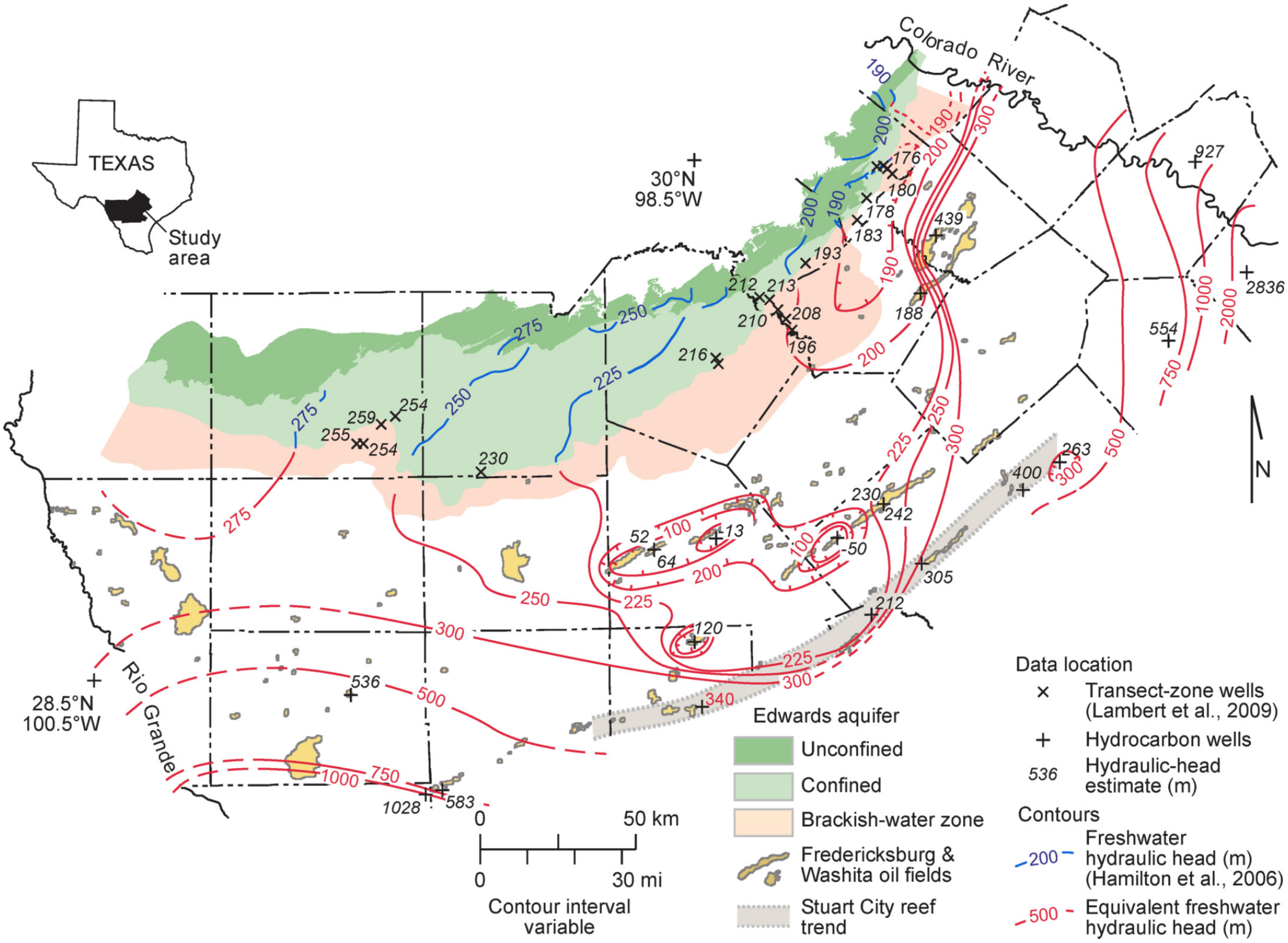

Figure 7. Map of potentiometric surface for the Edwards Group using (a) equivalent freshwater head for freshwater zone and updip brackish-water zone and (b) point-water head for downdip saline zone. Point-water hydraulic head uses variable ρ_w in Equations 7–9. Variable contour interval selected to merge equipotential lines in freshwater zone with those in brackish- and saltwater zones. 1 m = ~3.28 ft.

(3) How does Mixing of Water Occur in the Brackish-Water and Saltwater Zones?

There must be a hydrologic process to bring freshwater and saline water together for them to be mixed in the Edwards Group. The complex vertical interfingering of fresh and saline waters across the brackish zone (Schultz, 1993; Hovorka et al., 1998; Lambert et al., 2010) is hypothesized to result from convergence of flow. Groundwater in the freshwater part of the aquifer is moved by gravitational drive from the recharge area toward, and locally past, the area mapped under the bad-water line (Hamilton et al., 2006; Brakefield et al., 2015). A reversal in gradient in hydraulic head somewhere downdip (Figs. 6 and 7) and the presence of high fluid pressure at depth (Fig. 5) indicate that updip-directed lateral transport of saline water (Fig. 4) toward the brackish-water zone is possible.

The main mechanism creating variation in salinity across the brackish-water and saltwater zones might be transient and hysteretic displacement. An analogy of hydrodynamic mixing of freshwater and seawater in coastal areas and oceanic islands may be useful. The brackish-water zone of the Edwards aquifer would reflect dispersion between converging freshwater and saltwater taking place over a range of displacement periods. Variation in recharge rate within and between the Pleistocene and Holocene epochs (Loáiciga et al., 2000), e.g., on a time scale of 5−100 ka, would change the position of the interface between freshwater and saltwater. Tectonic uplift and downcutting of coastal streams on a time scale of 100 ka–1 Ma (Galloway, 1982) might have episodically increased the hydraulic-head gradient and depth of meteoric circulation, displacing saltwater, and pushing the bad-water line to greater depth. The updip-directed flux of brine from a geopressured zone could have changed because of (1) episodic nature of pressure buildup and fault release of fluid, and (2) progressive decay of the magnitude of geopressure and consequent decreased frequency of discharge episodes (Jones, 1975; Leftwich and Engelder, 1994; Harrison and Summa, 1991). In a transient system, the interface between the various fluids moves back and forth at different time scales, depending on the respective fluxes driving the fluids. Because of dispersion, displacement during each cycle is incomplete.

Mixing has an especially complex affect on TDS where multiple groundwaters having different salinities are involved. Upward-directed discharge of saline water from the Trinity Group, possibly focused along the Karnes-Atascosa Fault Zone, would change the salinity of brine moving updip in the Edwards Group from the Stuart City Reef Trend. The apparent ‘freshening’ of Edwards groundwater in the updip direction across the saline zone might be explained if TDS of groundwater from the Trinity Group is lower than TDS of geopressured brine entering the Edwards Group farther downdip.

The brackish-water zone all but disappears in the vicinity of Comal and San Marcos springs (Fig. 4) (Johnson and Schindel, 2008; Brakefield et al., 2015). At the east-northeast side of the study area between the Comal and San Marcos springs, the width of the confined aquifer is typically <3.5 km (<2 mi) (Fig. 1). Steep gradient in salinity across faults suggests little mixing of freshwater and saltwater. Faults that act as a barrier to flow might limit the depth of freshwater circulation, which allows saltwater to migrate farther updip.

Across the San Marcos Arch westward toward the Devils River Trend, however, a greater downdip flux of freshwater, relative to the updip flux of saltwater, and greater cumulative mixing between freshwater and saltwater could account for: (1) greater width (30−50 km [18−22 mi]) of the freshwater aquifer, (2) broader brackish-water zone, and (3) a less steep salinity gradient across the brackish-water zone (~600 mg/L/km [~966 mg/L/mi]). This area also has higher matrix permeability than the area to the northeast (Hovorka et al., 1995), perhaps reflecting a greater degree of freshwater-saltwater mixing across a shifting convergence zone. Additional study is needed to better understand hydrogeologic control of the position of the bad-water line westward across the San Marcos Arch toward the Devils River Trend. Its control, however, might be partly related to fault alignment relative to groundwater flow path, fault density, and fault displacement.

4. What are Implications of Convergent Mixing for Cross-Formational Flow across the Edwards Aquifer?

Convergent flow of freshwater and saltwater suggests there could be a significant amount of vertical, cross-formational discharge. Interpreted closure of some hydraulic-head contours along the brackish-water zone (Fig. 6) implies there must be vertical cross-formational flux. Previous numerical models of the water resources of the Edwards aquifer have been calibrated without including vertical upward-directed discharge out of the Edwards aquifer (Lindgren et al., 2004; Brakefield et al., 2015; Fratesi et al., 2015). Vertical flow from the Trinity aquifer upward into the Edwards Group, however, has been included in models.

Vertical cross-formational flow is a typical component of regional-scale flow in confined aquifers. In most confined aquifers it is how recharged water exits a flow system. Because models have been calibrated without including vertical flow, it might be a small percentage of the overall water budget of the Edwards aquifer. Leaving upward-directed discharge out of a model, however, could hide error in other water-budget terms. Including upward-directed discharge might allow greater recharge rates, whether from stream loss or from vertical influx from the underlying Trinity aquifer. The magnitude of the error could vary across the aquifer. The spatial distribution of vertical flow of groundwater across the Lower and Upper Cretaceous sections is unknown. It might be different in the freshwater, brackish-water, and saline parts of the aquifer.

CONCLUSIONS

While additional data and study are needed to confirm the findings of this study, convergent flow between hydropressured and geopressured regimes, transporting freshwater and saltwater, respectively, most likely accounts for the origin and distribution of the brackish-water zone in the Edwards aquifer. This is supported by maps of TDS and of freshwater hydraulic head that were drawn by pooling data from the groundwater and petroleum industries.

The presence of geopressure conditions in the deep Edwards Group is indicated by fluid-pressure data from oil and gas wells, but has not been verified using field information. Geopressure in the superjacent Cenozoic section might have induced high fluid pressure in the Edwards Group. A regime of geopressure or 'subgeopressure' within the Edwards Group, however, seems required to drive saltwater updip toward the freshwater zone and to account for high hydraulic head in fault-bounded saline rocks adjacent to the freshwater aquifer.

This study extended the Schultz (1992, 1993) calibration between TDS and log resistivity to TDS >200,000 mg/L (Fig. 3). The log-linear regression for Schultz (1993) data lies within the confidence interval of the pooled data regression. The so-called bad-water line drawn in this study is consistent with downdip saline data and with recent data on chemical composition samples of brackish water and downdip freshwater. The 1000 mg/L TDS line slightly differs from that of Schultz (1992, 1993), which was drawn to include the maximum lateral extent of freshwater-bearing intervals in the aquifer.

Future studies should consider vertical cross-formational flow across the Edwards aquifer. Cross-formational discharge is typical of confined aquifers and can account for a significant part of a water budget. Vertical discharge is implied by closed equipotential contours that are obvious when hydraulic-head data from the freshwater and saline sections are pooled.

Convergent flow of fresh and saline water from hydropressured and geopressured systems also has been suggested for the Carrizo-Wilcox aquifer in Central Texas (Dutton et al., 2006). Other aquifers beneath the upper coastal plain in the western Gulf of Mexico, including but not limited to the Queen City and Sparta aquifers (Kelley et al., 2004), have a similar downdip increase in TDS with brackish- and saline-water zones. It seems likely that regional distribution in hydraulic head and salinity in these aquifer systems would be explained by a similar process of convergent flow. Accounting for the convergent-flow process might improve calibration and predictive capability of regional models of groundwater flow and water resources in these coastal aquifers.

ACKNOWLEDGMENTS

Allen Clarke (U.S. Geological Survey) and Mike Younger (Blackbrush Energy) helped identify the Edwards Group in borehole geophysical logs. Mike Younger also provided historical context for oil and gas production in Edwards reservoirs. Jerry Lucia (UT Bureau of Economic Geology) assisted with capillarity and pressure calculations. H. Scott Hamlin (UT Bureau of Economic Geology) provided background information on converting resistivity to TDS.

REFERENCES CITED

Ahmed, T., 2006, Reservoir engineering handbook, 3rd ed.: Elsevier Publishing, Burlington, Massachusetts, 1360 p., doi:10.1016/b978-0-7506-7972-5.x5000-5.

Archie, G. E., 1942, The electrical resistivity log as an aid in determining some reservoir characteristics: Journal of Petroleum Technology, v. 5, p. 54–62, doi:10.2118/942054-g.

Arroyo, J. A., ed., 2004, The future of desalination in Texas—Technical papers, case studies, and desalination technology resources, v. 2, biennial report on seawater desalination: Texas Water Development Board Report 363, Austin, variably paginated.

Asquith, G. B., and D. A. Krygowski, 2004, Basic well log analysis, 2nd ed.: American Association of Petroleum Geologists Methods in Exploration Series 16, Tulsa, Oklahoma, 244 p.

Bachu, S., 1995, Flow of variable-density formation water in deep sloping aquifers: Review of methods of representation with case studies: Journal of Hydrology, v. 164, p. 19−38, doi:10.1016/0022-1694(94)02578-y.

Bair, E. S., T. P. O'Donnell, and L. W. Picking, 1985; Potentiometric mapping from incomplete drill-stem test data: Palo Duro Basin area, Texas and New Mexico: Ground Water, v. 23, p. 198−211, doi:10.1111/j.1745-6584.1985.tb02793.x.

Bebout, D. G., and R. G. Loucks, 1974, Stuart City Trend, Lower Cretaceous, South Texas: A carbonate shelf-margin model for hydrocarbon exploration: Texas Bureau of Economic Geology Report of Investigations, p. 78−80, doi:10.23867/ri0078d.

Belitz, K., and J. D. Bredehoeft, 1988; Hydrodynamics of Denver Basin: Explanation of subnormal fluid pressures: American Association of Petroleum Geologists Bulletin, v. 72, p. 1334−1359, doi:10.1306/703c999c-1707-11d78645000102c1865d.

Bethke, C. M., 1986, Inverse hydrologic analysis of the distribution and origin of Gulf Coast−type geopressured zones: Journal of Geophysical Research, v. 91, p. 6535−6545, doi:10.1029/jb091ib06p06535.

Billingsley, L., B. Layton, and L. Finger, 2016, Geoscience applications to economic development of a relatively shallow, low gravity, structurally complex Eagle Ford oil development, Atascosa County, Texas: Gulf Coast Association of Geological Societies Transactions, v. 66, p. 53–61.

Blondes, M. S., K. D. Gans, J. J. Thordsen, M. E. Reidy, B. Thomas, M. A. Engle, Y. K. Kharaka, and E. L. Rowan, 2013, U.S. Geological Survey National Produced Waters Geochemical Database, v. 2.1 (provisional): <http://energy.usgs.gov/EnvironmentalAspects/EnvironmentalAspectsofEnergyProductionandUse/ProducedWaters.aspx#3822349-data> Accessed November 2015.

Brakefield, L. K., J. T. White, N. A. Houston, and J. V. Thomas, 2015, Updated numerical model with uncertainty assessment of 1950−56 drought conditions on brackish-water movement within the Edward aquifer, San Antonio, Texas: U.S. Geological Survey Scientific Investigations Report 2015−5081, 66 p., <https://pubs.usgs.gov/sir/2015/5081/sir2015-5081.pdf> Last accessed July 26, 2017.

Draeger, D., 2016, Aquifer storage recovery ASR at New Braunfels airport: Presentation made to City Council Workshop, New Braunfels, Texas, June 27, 2016, 18 p., <http://www.nbutexas.com/LinkClick.aspx?fileticket=nsToNUgfZQI%3D&portalid=11> Accessed June 22, 2017.

Dutton, A. R., J. P. Nicot, and K. S. Kier, 2006, Hydrodynamic convergence of hydropressured and geopressured zones, Central Texas, Gulf of Mexico Basin, USA: Hydrogeology Journal, v. 14, p. 859−867, doi:10.1007/s10040-006-0024-5.

Evamy, B. D., 1967, Dedolomitization and development of rhombohedral pores in limestones: Journal of Sedimentary Petrology, v. 37, p. 1204−1215, doi:10.1306/74D71870-2B21-11D7-8648000102C1865D.

Ewing, T. E., 1990, Tectonic map of Texas: Texas Bureau of Economic Geology, Austin, scale 1:750,000.

Ewing, T. E., 1991, Structural framework, *in* A. Salvador, ed., The geology of North America, v. J: The Gulf of Mexico Basin: Geological Society of America, Boulder, Colorado, p. 31−52, doi:10.1130/dnag-gna-j.31.

Ferrill, D. A., D. W. Sims, D. J. Waiting, A. P. Morris, N. M. Franklin, and A. L. Schultz, 2004, Structural framework of the Edwards aquifer recharge zone in south-central Texas: Geological Society of America Bulletin, v. 116, p. 407–418, doi:10.1130/b25174.1.

Fratesi, S. E., R. T. Green, F. P. Bertetti, R. N. McGinnis, N. Toll, H. Başağaoğlu, L. Gergen, J. Winterle, Y. Cabeza, and J. Carrera, 2015, Development of a finite-element method groundwater flow model of the Edwards aquifer: Final Report prepared for the Edwards Aquifer Authority by Southwest Research Institute under SwRI Project 20–17344, San Antonio, 180 p.

Galloway, W. E., 1982, Epigenetic zonation and fluid flow history of uranium-bearing fluvial aquifer systems, South Texas uranium province: Texas Bureau of Economic Geology Report of Investigations 119, Austin, 31 p.

Galloway, W. E., D. K. Hobday, and K. Magara, 1982, Frio formation of Texas Gulf Coastal Plain: Depositional systems, structural framework, and hydrocarbon distribution: American Association of Petroleum Geologists Bulletin, v. 66, p. 649–688, doi:10.1306/03b5a2f5-16d1-11d7-8645000102c1865d.

Galloway, W. E., T. E. Ewing, C. M. Garret, N. Tyler, and D. G. Bebout, 1983, Atlas of major Texas oil reservoirs: Texas Bureau of Economic Geology, Austin, 139 p., 5 plates, doi:10.23867/at0002d.

Galloway, W. E., 2001, Cenozoic evolution of sediment accumulation in deltaic and shore-zone depositional systems, northern Gulf of Mexico Basin: Marine and Petroleum Geology, v. 18, p. 1031−1040, doi:10.1016/s0264-8172(01)00045-9.

GEOMAP, Inc., 1979, Executive reference map no. 313 for south central Texas: Plano, Texas, scale 1:250,000.

George, P. G., R. E. Mace, and R. Petrossian, 2011, Aquifers of Texas: Texas Water Development Board Report 380, Austin, 172 p.

Goh, P. S., A. F. Ismail, and N. Hilal, 2016, Recent trends in membranes and membrane processes for desalination: Desalination, v. 391, p. 43−60, doi:10.1016/j.desal.2015.12.016.

Groschen, G. E., 1994, Analysis of data from test-well sites along the downdip limit of freshwater in the Edwards aquifer, San Antonio, Texas, 1985−87: U.S. Geological Survey Water-Resources Investigations Report 93−4100, 98 p., <https://pubs.usgs.gov/wri/1993/4100/report.pdf> Last accessed July 26, 2017.

Groschen, G. E., and P. M. Buszka, 1997, Hydrologeologic framework and geochemistry of the Edwards aquifer saline-water zone, south-central Texas: U.S. Geological Survey Water-Resources Investigations Report 97−4133, 54 p. <https://pubs.usgs.gov/wri/1997/4113/report.pdf> Last accessed July 26, 2017.

Hamilton, J. M., R. Esquilin, and G. M. Schindel, 2006, Edwards Aquifer Authority Synoptic Water Level Program 1999−2004 Report: Edwards Aquifer Authority Report 06−01, San Antonio, Texas, 120 p.

Hamlin, H. S., and L. de la Rocha, 2015, Using electric logs to estimate groundwater salinity and map brackish groundwater resources in the Carrizo-Wilcox aquifer in South Texas: Gulf Coast Association of Geological Societies Journal, v. 4, p. 109−131, <http://www.gcags.org/Journal/2015.GCAGS.Journal/2015.Journal.v4.7.p109-131.Hamlin.and.de.la.Rocha.press.pdf> Last accessed July 26, 2017.

Harrison, W. J., and L. L. Summa, 1991, Paleohydrology of the Gulf of Mexico Basin: American Journal of Science, v. 291, p. 109−176, doi:10.2475/ajs.291.2.109.

Hoff, S. Z., Jr., 2016, The development of a conceptual model to describe the occurrence of brackish water in the Edwards aquifer, south-central Texas: Master's Thesis, University of Texas at San Antonio, 66 p.

Hovorka, S. D., A. R. Dutton, S. C. Ruppel, and J. Yeh, 1994, Sedimentologic and diagenetic controls on aquifer properties, Lower Cretaceous Edwards carbonate aquifer, Texas: Implications for aquifer management: Gulf Coast Association of Geological Societies Transactions, v. 44, p. 277−284.

Hovorka, S. D., R. E. Mace, and E. W. Collins, 1995, Regional distribution of permeability in the Edwards aquifer: Gulf Coast Association of Geological Societies Transactions, v. 45, p. 259−265.

Hovorka, S. D., A. R. Dutton, S. C. Ruppel, and J. Yeh, 1996, Edwards aquifer ground-water resources: Geologic controls on porosity development in platform carbonates, South Texas: Texas Bureau of Economic Geology Report of Investigations 238, Austin, 75 p., doi:10.23867/ri0238d.

Hovorka, S. D., R. E. Mace, and E. W. Collins, 1998, Permeability structure of the Edwards aquifer, South Texas—Implications for aquifer management: Texas Bureau of Economic Geology Report of Investigations 250, Austin, 55 p., doi:10.23867/ri0250d.

Hovorka, S. D., T. Phu, J. P. Nicot, and A. L. Lindley, 2004, Refining the conceptual model for flow in the Edwards aquifer—Characterizing the role of fractures and conduits in the Balcones Fault Zone segment: Final Contract Report to the Edwards Aquifer Authority, San Antonio, Texas, prepared by the Texas Bureau of Economic Geology, Austin, 53 p.

Jackson, M. P. A., 1982, Fault tectonics of the East Texas Basin: Texas Bureau of Economic Geology Geological Circular 82−4, Austin, 31 p., doi:10.23867/gc8204d.

Jagnow, D. H., C. A. Hill, D. G. Davis, H. R. DuChene, K. I. Cunningham, D. E. Northup, and J. M. Queen, 2000, History of sulfuric acid theory of speleogenesis in the Guadalupe Mountains, New Mexico: Journal of Cave and Karst Studies, v. 62, no. 2, p. 54−59.

Johnson, S. B., and G. M. Schindel, 2008, Evaluation of the option to designate a separate San Marcos pool for critical period management: Edwards Aquifer Authority Report 08−01, San Antonio, Texas, 109 p.

Jones, I. C., R. Anaya, and S. Wade, 2011, Groundwater availability model for the Hill Country portion of the Trinity aquifer system, Texas: Texas Water Development Board Report 377, Austin, 165 p.

Jones, P. H., 1975, Geothermal and hydrocarbon regimes, northern Gulf of Mexico Basin, *in* M. H. Dorfman and R. W. Deller, eds., Proceedings of the First Geopressured Geothermal Energy Conference: University of Texas at Austin Center for Energy Studies, p. 15−89.

Jones, P. H., and R. H. Wallace, Jr., 1974, Hydrogeologic aspects of structural deformation in the northern Gulf of Mexico Basin: U.S. Geological Survey Journal of Research, v. 2, p. 511−517.

Karagiannis, I., and P. G. Soldatos, 2008, Water desalination cost literature: Review and assessment: Desalination, v. 223, p. 448−456, doi:10.1016/j.desal.2007.02.071.

Kelley, V. A., N. E. Deeds, D. G. Fryar, J. P. Nicot, J. L. Jones, A. R. Dutton, G. Bruehl, T. Unger-Holtz, and J. L. Machin, 2004, Groundwater availability models for the Queen City and Sparta aquifers: Final Report prepared for the Texas Water Development Board by Intera, Inc., Austin, variably paginated.

Kosters, E. C., D. G. Bebout, S. J. Seni, C. M. Garrett, L. F. Brown, Jr., H. S. Hamlin, S. P. Dutton, S. C. Ruppel, R. J. Finley, and N. Tyler, 1989, Atlas of major Texas gas reservoirs: Texas Bureau of Economic Geology, Austin, 161 p., 4 plates.

Kreitler, C. W., 1989, Hydrogeology of sedimentary basins: Journal of Hydrology, v. 106, p. 29−53, doi:10.1016/0022-1694(89)90165-0.

Lambert, R. B., A. G. Hunt, G. P. Stanton, and M. B. Nyman, 2009, Water-level, borehole geophysical log, and water-quality data from wells transecting the freshwater/saline-water interface of the San Antonio segment of the Edwards aquifer, south-central Texas, 1999−2007, U.S. Geological Survey Data Series 403, 9 p., <https://pubs.usgs.gov/ds/403/pdf/ds403.pdf> Last accessed July 26, 2017.

Lambert, R. B., A. G. Hunt, G. P. Stanton, and M. B. Nyman, 2010, Lithologic and physicochemical properties and hydraulics of flow in and near the freshwater/saline-water transition zone, San Antonio segment of the Edwards aquifer, south-central Texas, Based on water-level and borehole geophysical log data, 1999–2007: U.S. Geological Survey Scientific Investigations Report 2010–5122, 69 p., <https://pubs.usgs.gov/sir/2010/5122/> Last accessed July 26, 2017.

Land, L. S., and D. R. Prezbindowski, 1981, The origin and evolution of saline formation water, Lower Cretaceous carbonates, south-central Texas, U.S.A: Journal of Hydrology, v. 54, p. 51−74, doi:10.1016/0022-1694(81)90152-9.

Land, L. S., and G. L. Macpherson, 1992, Origin of saline formation waters, Cenozoic section, Gulf of Mexico sedimentary basin: American Association of Petroleum Geologists Bulletin, v. 76, p. 1344−1362, doi:10.1306/bdff89e8-1718-11d7-8645000102c1865d.

Lasser Production Data Inc., 2015, Texas LPD production database, <http://www.lasserdata.com> Accessed February, 2016.

Leftwich, J. T., Jr., and T. Engelder, 1994, The characteristics of geopressure profiles in the Gulf of Mexico Basin, *in* P. J. Ortoleva, ed., Basin compartments and seals: American Association of Petroleum Geologists Memoir 61, Tulsa, Oklahoma, p. 119−130.

Lindgren, R. J., A. R. Dutton, S. D. Hovorka, S. R. H. Worthington, and S. Painter, 2004, Conceptualization and simulation of the Edwards aquifer, San Antonio region, Texas: U.S. Geological Survey Scientific Investigations Report 2004−5277, 143 p., <https://pubs.usgs.gov/sir/2004/5277> Last accessed July 26, 2017.

Loáiciga, H. A., D. R. Maidment, and J. B. Valdes, 2000, Climate-change impacts in a regional karst aquifer, Texas, USA: Journal of Hydrology, v. 227, p. 173–194, doi:10.1016/s0022-1694(99)00179-1.

Lozo, F. E., and C. I. Smith, 1964, Revision of Comanche Cretaceous stratigraphic nomenclature, southern Edwards Plateau, southwest Texas: Gulf Coast Association of Geological Societies Transactions, v. 14, p. 285−307.

Lusczynski, N. J., 1961, Head and flow of ground water of variable density: Journal of Geophysical Research, v. 66, p. 4247–4256, doi:10.1029/JZ066i012p04247.

Lyons, W. C., and G. S. Plisga, eds., 2004, Standard handbook of petroleum and natural gas engineering, 2nd ed.: Elsevier, Boston, Massachusetts, variably paginated, doi:10.1016/b978-0-7506-7785-1.x5011-8.

Maclay, R. W., 1995, Geology and hydrology of the Edwards aquifer in the San Antonio area, Texas: U.S. Geological Survey Water-Resources Investigations Report 95−4186, 64 p., <https://pubs.usgs.gov/wri/1995/4186/report.pdf> Last accessed July 26, 2017.

Maclay, R. W., and T. A. Small, 1984, Carbonate geology and hydrology of the Edwards aquifer in the San Antonio area, Texas: Gulf Coast Association of Geological Societies Transactions, v. 14, p. 253−261.

McNeal, R. P., 1965, Hydrodynamics of the Permian Basin, *in* A. Young and J. Galley, eds., Fluids in subsurface environments: American Association of Petroleum Geologists Memoir 4, Tulsa, Oklahoma, p. 308−326.

Mench-Ellis, P. M., 1985, Diagenesis of the Lower Cretaceous Edwards group in the Balcones Fault Zone area, south-central Texas: Ph.D. Dissertation, University of Texas at Austin, 326 p.

NOAA, 2016, Local south central Texas climate information: National Weather Service Weather Forecast Office, Silver Spring, Maryland, <http://www.weather.gov/ewx/> Accessed April, 2016.

Oetting, G. C., J. L. Banner, and J. M. Sharp, Jr., 1996, Regional controls on the geochemical evolution of saline groundwaters in the Edwards aquifer, Central Texas: Journal of Hydrology, v. 181, p. 251−283, doi:10.1016/0022-1694(95)02906-010.1016/0022-1694(95)02906-0.

Pavlicek, D., T. A. Small, and P. L. Rettman, 1987, Hydrogeologic data from a study of the freshwater zone/saline water zone interface in the Edwards aquifer, Central Texas: U.S. Geological Survey Open-File Report 87−389, 108 p., <https://pubs.usgs.gov/of/1987/0389/report.pdf> Last accessed July 26, 2017.

Pearson, F. J., Jr., and P. L. Rettman, 1976, Geochemical and isotopic analyses of waters associated with the Edwards limestone aquifer, Central Texas: U.S. Geological Survey Report for the Edwards Underground Water District, San Antonio, Texas, 35 p., <https://www.edwardsaquifer.org/documents/1976_Pearson Rettman_Geochemical-IsotopicAnalyses.pdf> Last accessed July 26, 2017.

Post, V., H. Kooi, and C. Simmons, 2007, Using hydraulic head measurements in variable-density ground water flow analyses: Ground Water, v. 45, p. 664−671, doi:10.1111/j.1745-6584.2007.00339.x.

Prezbindowski, D. R., 1981, Carbonate rock-water diagenesis lower Cretaceous, Stuart City Trend, South Texas: Ph.D. Dissertation, University of Texas at Austin, 236 p.

Rose, P. R., 1972, Edwards Group, surface and subsurface, Central Texas: Texas Bureau of Economic Geology Report of Investigations 74, Austin, 198 p., doi:10.23867/ri0074d.

Schindel, G. M., and M. Gary, in press, The Balcones Fault Zone segment of the Edwards aquifer of south-central Texas, *in* K. W. Stafford, ed., Hypogene karst of Texas: Texas Speleological Survey, Austin.

Schlumberger, 1974, Log interpretation, vol. II—Applications: Schlumberger Limited, New York, New York, 116 p.

Schultz, A. L., 1992, Using geophysical logs in the Edwards aquifer to estimate water quality along the freshwater/saline-water interface (Uvalde to San Antonio, Texas): Edwards Underground Water District Report 92−03, San Antonio, Texas, 47 p.

Schultz, A. L, 1993, Defining the Edwards aquifer freshwater/saline-water interface with geophysical logs and measured data (San Antonio to Kyle, Texas): Edwards Underground Water District Report 93−06, San Antonio, Texas, 81 p.

Sharp, J. M., Jr., 1990, Stratigraphic, geomorphic and structural controls of the Edwards aquifer, Texas, U.S.A., *in* E. S. Simpson, and J. M. Sharp, Jr., eds., Selected papers from the 28th International Geological Congress v. 1: International Association of Hydrogeologists, Heise, Hannover, Germany, p. 67−82.

Thomas, J. V., G. P. Stanton, and R. B. Lambert, 2012, Borehole geophysical, fluid, and hydraulic properties within and surrounding the freshwater/saline-water transition zone, San Antonio segment of the Edwards aquifer, south-central Texas, 2010–11: U.S. Geological Survey Scientific Investigations Report 2012−5285, 77 p., <https://pubs.usgs.gov/sir/2012/5285> Last accessed July 26, 2017.

Turcan, A. N., Jr., 1966, Calculation of water quality from electrical logs—Theory and practice: Louisiana Geological Survey Water Resources Pamphlet 19, Baton Rouge, 23 p.

TWDB, 2016a, Water levels by aquifer: Texas Water Development Board, Austin, <http://www.twdb.texas.gov/groundwater/data/gwdbrpt.asp> Accessed January, 2016.

TWDB, 2016b, Water quality by aquifer: Texas Water Development Board, Austin, <http://www.twdb.texas.gov/groundwater/data/gwdbrpt.asp> Accessed January, 2016.

USGS, 2013, NED (National Elevation Data) for South Texas—1/3 arc-second NAVD1988, <https://viewer.nationalmap.gov/basic/#productSearch> Accessed March, 2015.

Worthington, S. R., 2003, Conduits and turbulent flow in the Edwards aquifer: Contract Report prepared for Edwards Aquifer Authority, San Antonio, Texas, 42 p.